Swift-Hohenberg model for magnetoconvection

S. M. Cox, P. C. Matthews, and S. L. Pollicott
School of Mathematical Sciences, University of Nottingham, University Park, Nottingham NG7 2RD, United Kingdom
(Received 19 August 2003; revised manuscript received 25 March 2004; published 22 June 2004)

A model system of partial differential equations in two dimensions is derived from the three-dimensional equations for thermal convection in a horizontal fluid layer in a vertical magnetic field. The model consists of an equation of Swift-Hohenberg type for the amplitude of convection, coupled to an equation for a large-scale mode representing the local strength of the magnetic field. The model facilitates both analytical and numerical studies of magnetoconvection in large domains. In particular, we investigate the phenomenon of flux separation, where the domain divides into regions of strong convection with a weak magnetic field and regions of weak convection with a strong field. Analytical predictions of flux separation based on weakly nonlinear analysis are extended into the fully nonlinear regime through numerical simulations. The results of the model are compared with simulations of the full three-dimensional magnetoconvection problem.

DOI: 10.1103/PhysRevE.69.066314 PACS number(s): 47.54.+r, 47.20.Bp, 47.27.Te, 47.20.Lz

I. INTRODUCTION

Heat transfer in the convection zone of the Sun is influenced by the interaction of the motion of the plasma with the Sun's magnetic field. Regions of intense magnetic field, such as sunspots, resist the fluid motion and hence reduce convective heat transport, while the fluid motion itself may rearrange or intensify the magnetic field. This complex interaction provides the motivation for the study of magnetoconvection, where thermal convection of an electrically conducting fluid takes place in a plane layer threaded by a vertical magnetic field. This problem has been widely studied and yields a wide range of interesting dynamical phenomena [1–8].

Numerical simulations of magnetoconvection in regions of large horizontal extent exhibit a phenomenon known as flux separation, where the convection cells and magnetic field rearrange spontaneously into areas where there is vigorous convection and weak magnetic field and other areas where the magnetic field is strong and the convection is reduced [5,9,10]. In its most extreme form, this process leads to the formation of "convectons" [11,12], which are isolated, stationary convection cells surrounded by practically stationary regions of strong magnetic field. Convectons can easily be found in two-dimensional simulations; while they can also be found in three dimensions, the behavior in that case is typically more complicated and unsteady (see [11,12] and the simulations in Sec. III below).

The physical mechanism for flux separation is a straightforward feedback process: regions of slightly weaker magnetic field lead to stronger convection, and stronger convection cells are more effective at expelling magnetic field. This process is resisted only by the diffusion of magnetic field, which is weak over large horizontal scales. A quantitative calculation of the circumstances under which flux separation may develop was given by Matthews and Cox [7,13], by considering the stability of small-amplitude two-dimensional convection rolls near the onset of convection, under "ideal" boundary conditions. They began by noting a crucial feature of magnetoconvection, which is that the total flux of the magnetic field through the layer is a conserved quantity, and this leads to a large-scale neutral mode representing rearrangement of the magnetic field. Near the onset of convection, the usual Ginzburg-Landau equation for the amplitude of convection rolls must be coupled to this large-scale mode: analysis of this coupled pair of equations then leads to the conclusion that all convection rolls can be made unstable near onset to an amplitude modulation on large horizontal scales. This instability occurs for small values of the magnetic diffusivity and moderate values of the imposed magnetic field [13]. Of course, such an idealized analysis of convection near onset cannot be applied directly to the numerical simulations of strongly nonlinear, compressible magnetoconvection [5,10], but it may help to suggest parameter regimes for future numerical studies.

A significant hindrance to three-dimensional numerical simulations is that such computations are expensive, because flux separation occurs only in a large domain and can also require a long integration time for the instability to develop. Since (discounting geometrical parameters) there are four dimensionless parameters in the problem, it is not possible to carry out a significant survey of parameter space using full three-dimensional simulations.

Our aim in this paper is to develop a reduced two-dimensional model for magnetoconvection in a horizontal fluid layer, in which the equations are averaged in the vertical direction. Such reduced models have been widely used for other convection problems, the original example being that of Swift and Hohenberg [14], where the three-dimensional equations for thermal convection are reduced to a single partial differential equation in two horizontal space dimensions. For stress-free boundaries, a horizontal mean flow is only weakly damped on large horizontal scales, and this mean flow plays an important role in some of the instabilities of convection rolls. Manneville [15] derived a model in which the stream function for this large-scale flow is coupled to a Swift-Hohenberg equation. Closely related models have also been derived for rotating convection, at infinite Prandtl number [16], and at finite Prandtl number [17] and used to investigate the small-angle and Küppers-Lortz instabilities of convection rolls [18,19]. For magnetoconvection, such models have not yet been derived, although

a two-dimensional system of 11 equations has been obtained by a modal truncation of the governing equations [12]. Our derivation below results in just two equations, describing the amplitude of convection and the magnitude of the vertical magnetic field.

We begin in Sec. II by summarizing the three-dimensional magnetoconvection problem from which our two-dimensional model is derived and some associated linear stability results. Numerical simulations of the full three-dimensional model are described in Sec. III; these illustrate the phenomenon of flux separation and allow later comparison with corresponding numerical results for the reduced model, which is derived in Sec. IV. The stability of magnetoconvection rolls according to both the full and reduced models is discussed in Sec. V, and the nonlinear evolution of the instability is analyzed in Sec. VI. Numerical simulations of the reduced model are presented in Sec. VII.

II. GOVERNING EQUATIONS AND LINEAR THEORY FOR MAGNETOCONVECTION

The dimensionless governing equations for incompressible magnetoconvection are

$$\frac{1}{\sigma}\left[\frac{\partial \boldsymbol{u}}{\partial t}+\boldsymbol{u}\cdot\boldsymbol{\nabla}\boldsymbol{u}\right]=-\boldsymbol{\nabla}P+R\theta\hat{z}+\zeta Q\frac{\partial \boldsymbol{B}}{\partial z}+\zeta Q\boldsymbol{B}\cdot\boldsymbol{\nabla}\boldsymbol{B}+\nabla^2\boldsymbol{u}, \tag{1}$$

$$\frac{\partial \theta}{\partial t}+\boldsymbol{u}\cdot\boldsymbol{\nabla}\theta=w+\nabla^2\theta, \tag{2}$$

$$\frac{\partial \boldsymbol{B}}{\partial t}=\boldsymbol{\nabla}\times(\boldsymbol{u}\times\boldsymbol{B})+\frac{\partial \boldsymbol{u}}{\partial z}+\zeta\nabla^2\boldsymbol{B}, \tag{3}$$

$$\boldsymbol{\nabla}\cdot\boldsymbol{u}=0,\quad \boldsymbol{\nabla}\cdot\boldsymbol{B}=0. \tag{4}$$

Here $\boldsymbol{u}=(u,v,w)$ is the fluid velocity, θ is the temperature perturbation from the basic state temperature profile $1-z$, and $\boldsymbol{B}=(B_x,B_y,B_z)$ is the perturbation from the initial uniform vertical magnetic field $(0,0,1)$. Lengths are nondimensionalized with the depth of the layer, times with the thermal diffusion time, and $\boldsymbol{B}$ with the strength of the imposed magnetic field [3]. The dimensionless parameters are the Prandtl number σ, the magnetic Prandtl number ζ measuring the ratio of magnetic to thermal diffusivity, the Chandrasekhar number Q [1] proportional to the square of the imposed magnetic field, and the Rayleigh number R measuring the imposed temperature difference across the layer.

We adopt the usual "ideal" boundary conditions, which allow the linear eigenfunctions to be trigonometric [1]. The boundaries are stress free and maintained at a fixed temperature, and the magnetic field is constrained to remain vertical at the boundaries, so

$$w=\frac{\partial u}{\partial z}=\frac{\partial v}{\partial z}=\theta=B_x=B_y=0 \tag{5}$$

at $z=0$ and $z=1$. In the horizontal directions x and y, periodic boundary conditions are assumed.

The conditions for the onset of convection are obtained by linearizing the equations and introducing a horizontal wave number k [1]. The marginal curve, for stationary disturbances, takes the form

$$R_m(k)=\frac{a^2(Q\pi^2+a^4)}{k^2}, \tag{6}$$

where $a^2=\pi^2+k^2$. This curve has a minimum at a critical wave number k_c that satisfies

$$a_c^4(2k_c^2-\pi^2)=Q\pi^4, \tag{7}$$

where $a_c^2=\pi^2+k_c^2$. By eliminating Q between Eqs. (6) and (7), the critical Rayleigh number R_c may be written as

$$R_c=\frac{2a_c^6}{\pi^2}. \tag{8}$$

Correspondingly, the critical wave number is given in terms of R_c by

$$k_c^2=\left(\frac{\pi^2R_c}{2}\right)^{1/3}-\pi^2. \tag{9}$$

An explicit expression relating R_c and Q may be derived by using Eqs. (9) and (7); this leads to

$$Q=\frac{R_c}{\pi^2}\left[1-\left(\frac{R_{\mathrm{RB}}}{R_c}\right)^{1/3}\right], \tag{10}$$

where R_{RB} is the critical Rayleigh number for convection in the absence of a magnetic field:

$$R_{\mathrm{RB}}=\frac{27\pi^4}{4}.$$

The formula (10) is analogous to that obtained for the case of rotating convection [20]. Note that Eq. (10) can be inverted to give the critical Rayleigh number explicitly as

$$R_c=\frac{1}{3}R_{\mathrm{RB}}(A+1+A^{-1})+Q\pi^2(1+2A^{-1}), \tag{11}$$

where

$$A^3=1+\frac{4Q}{3\pi^2}+\frac{8Q^2}{27\pi^4}[1+(1+\pi^2/Q)^{1/2}]. \tag{12}$$

The model derived below holds near the onset of convection through a stationary bifurcation, and so in applying the model we shall need to ensure that this bifurcation precedes the onset of oscillatory convection. A detailed analysis of the relative positions of the stationary and oscillatory marginal curves has been given by Dangelmayr [21], and for completeness the relevant results are summarized here. For oscillatory onset, which applies if $\zeta<1$ and Q is sufficiently large [1], the formula analogous to Eq. (10) is

$$Q=\frac{\alpha R_c}{\pi^2}\left[1-\beta\left(\frac{R_{\mathrm{RB}}}{R_c}\right)^{1/3}\right], \tag{13}$$

where

$$\alpha = \frac{1+\sigma}{(\zeta+\sigma)\zeta} \quad \text{and} \quad \beta^3 = \frac{(\zeta+\sigma)(1+\zeta)}{\sigma}. \tag{14}$$

By comparing Eqs. (13) and (10), a useful explicit formula can be found to determine whether the onset of convection is steady or oscillatory, for given values of Q, ζ, and σ. The result is that the stationary bifurcation occurs first as R is increased if $Q<Q^*$, while the oscillatory bifurcation occurs first if $Q>Q^*$, where

$$Q^* = \frac{R_{\mathrm{RB}}\alpha(\beta-1)(\alpha\beta-1)^2}{\pi^2(\alpha-1)^3}. \tag{15}$$

At $Q=Q^*$, there is a codimension-2 mode interaction between the steady and oscillatory convection modes. The results of this paper concern the case $Q<Q^*$. Note that our expression for Q^* corrects a minor typographical error in Dangelmayr's equation (5.24) [21].

An important feature of magnetoconvection is that the total flux of magnetic field through a horizontal surface,

$$F_B = \int\int B_z \, dx \, dy, \tag{16}$$

where the integral is over the whole periodic domain, is a conserved quantity: $F_B=0$ for all time (recall that B_z is the perturbation to the vertical magnetic field). As discussed by Matthews and Cox [13], this conservation law leads to an eigenmode that is only weakly damped on large horizontal scales and therefore must be included in any analysis involving large domains. This mode corresponds to displacing magnetic field lines but keeping them vertical, so $B_z \propto \exp(i\boldsymbol{k}\cdot\boldsymbol{x}+\lambda t)$, with growth rate given by

$$\lambda = -\zeta k^2. \tag{17}$$

The coupling of this mode to the convective mode forms the basis of the reduced model derived in Sec. IV.

III. SIMULATIONS OF THREE-DIMENSIONAL MAGNETOCONVECTION

Because of the astrophysical motivation, most previous numerical simulations of magnetoconvection have been concerned with the case of a compressible fluid [4–6,10]. There have been very few three-dimensional numerical simulations of the Boussinesq equations (1)–(4); one example is the work of Cattaneo, Emonet, and Weiss [8], but this is concerned only with very large Rayleigh numbers.

In view of the lack of previous simulations and in order to provide comparison with the reduced model of Sec. IV, we present in this section some simulations of Eqs. (1)–(4) near the onset of convection. The numerical code is based on the convection code of [22], extended to include the magnetic field. The pseudospectral method is employed [23], using Fourier series for the horizontal directions and Chebyshev polynomials in the vertical direction, with fast transforms to switch between the spectral coefficients and the corresponding physical values on the spatial grid.

The first simulations shown here are for $\sigma=1$, $\zeta=0.6$, and $Q=100$. For these values of σ and ζ, $Q^*=137$, so according to Eq. (15) the stationary bifurcation occurs first as R increases. The critical Rayleigh number is $R_c=2654$ and the wave number is $k_c=3.70$. The values of Q and ζ are well within the region where convection rolls are unstable to amplitude modulation according to Matthews and Cox [13]. The size of the periodic box is chosen to be 10.18; this allows exactly six pairs of rolls with the critical wave number. The numerical resolution is 64 points in each horizontal direction and 25 points in the vertical direction; the initial condition is a small-amplitude random perturbation from the equilibrium state.

FIG. 1. Stable, stationary solutions for two-dimensional magnetoconvection, showing grayscale images of total magnetic field strength. Parameters are $\sigma=1,\zeta=0.6,Q=100$, and the Rayleigh and Nusselt numbers are (a) $R=2700,N=1.75$, (b) $R=2800,N=1.91$, (c) $R=3500,N=2.19$, (d) $R=4000,N=2.36$.

Simulations in two dimensions carried out for a range of values of R initially show a regular roll pattern, but this state is unstable and is replaced by a stationary state exhibiting flux separation. For $R=2800$ this stable state has two pairs of convection cells occupying approximately one-half the domain, while in the other half the fluid is almost stationary. These states are closely related to the isolated solutions known as "convectons" [11]. In the stationary region the magnetic field strength is approximately 1.8 times its initial value. The transition from periodic rolls to a flux-separated state involves a significant increase in the Nusselt number N (defined as the ratio of heat flux in the convective state to that in the conductive state), from $N=1.08$ to $N=1.91$. As R is increased, the proportion of the domain filled by convection rolls increases, and at $R=4000$ there is one narrow plug of intense magnetic field surrounded by convection cells. This sequence is shown in Fig. 1.

A three-dimensional simulation at $R=2700$ results in a stationary pattern that does not show flux separation (Fig. 2). The pattern shows a zigzag arrangement of convection rolls. Typically, zigzag instabilities occur when straight convection rolls are forced to have a wave number less than k_c, but this is not the case here. To check that this behavior is not a consequence of the domain size, further simulations were carried out for different domain sizes; in each case, essentially the same zigzag solution was found.

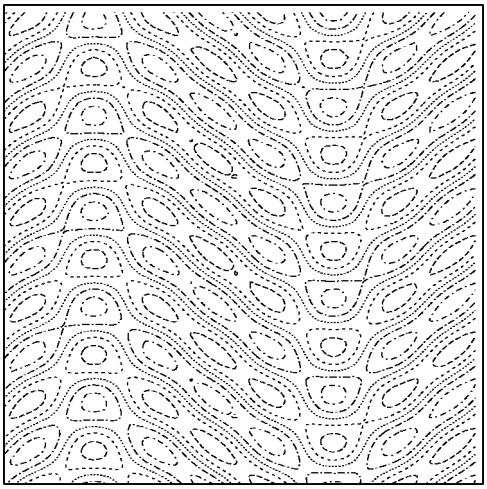

FIG. 2. Stable, stationary solution for three-dimensional magnetoconvection with $\sigma=1,\zeta=0.6,Q=100,R=2700$. The figure shows a contour plot of the vertical velocity w at the middle of the layer, at contour levels $-1,-0.5,0,0.5,1$.

For $R=2800$, the three-dimensional solution does exhibit strong flux separation, but the behavior is highly time dependent (Fig. 3). Less than half of the domain contains localized, vigorous, three-dimensional convection cells, while in the remainder the flow is very much weaker. The peak vertical velocity is approximately 15, but in the quiescent regions, the maximum vertical velocity is approximately 1 and the field strength is increased to 10%–20% above its initial value. The flow structure is constantly changing, but the snapshots of Fig. 3 show typical behavior. The Nusselt number fluctuates in the range 1.15–1.22.

Further simulations carried out for different values of R show a generally similar picture to that of Fig. 3. No stationary solutions showing flux separation were found. As R increases, flux separation becomes less clearly defined, as more and more of the domain is occupied by vigorous convection. Two-dimensional solutions such as those of Fig. 1 are unstable in three dimensions, exhibiting a rapid buckling along the axis of the rolls.

In order to provide a closer comparison with the two-dimensional model derived below, which has infinite Prandtl number, some further simulations were carried out with $\sigma=100$ and $Q=100$. However, for these parameter values the onset of magnetoconvection is oscillatory for $\zeta=0.6$, whereas the two-dimensional model assumes stationary onset. Therefore we take $\zeta=0.7$ instead, for which onset is indeed steady. In two dimensions, the results at $\sigma=100$ are very similar to those at $\sigma=1$: a sequence of results analogous to those shown in Fig. 1 was obtained as R increases. But in three dimensions the behavior at large σ is quite different. Results at $R=2800$ and $R=3000$ are shown in Fig. 4; in each case the behavior is unsteady but the figures show typical snapshots. Convection cells are less vigorous than at $\sigma=1$ and retain a roll-like structure locally. Modulation of the amplitude of convection is less pronounced than at $\sigma=1$, showing a variation of approximately a factor of 2 in the vertical velocity.

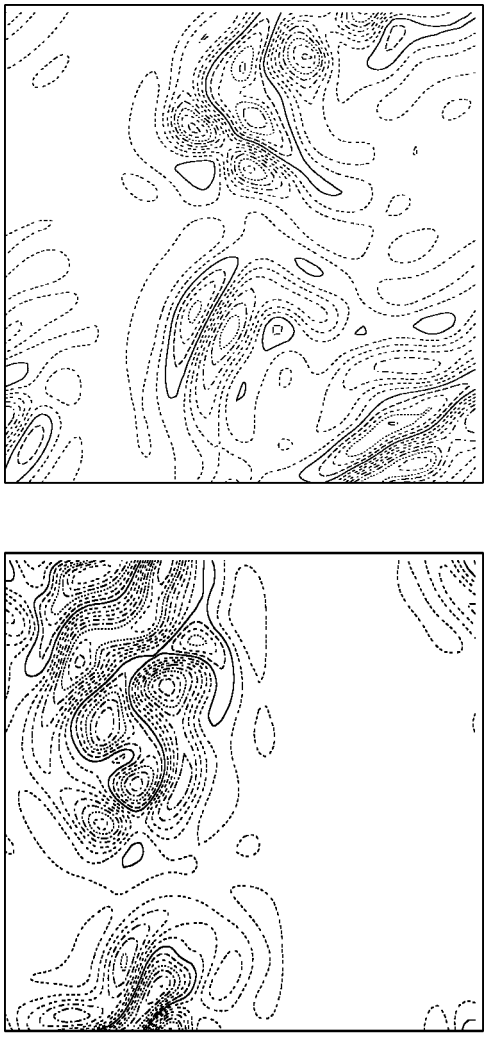

FIG. 3. Solutions for three-dimensional magnetoconvection with $\sigma=1,\zeta=0.6,Q=100,R=2800$. The figures show contour plots of the vertical velocity w at the middle of the layer, at contour levels -15, -13, …, 15. The two plots are separated by 10 time units.

IV. DERIVATION OF THE TWO-DIMENSIONAL MAGNETOCONVECTION MODEL

In this section, we introduce a reduced two-dimensional model for magnetoconvection in a Boussinesq fluid. Such models have been widely used for studying convection [14–17,19,24] and have the advantage of greatly simplifying both analytical and numerical studies, while capturing the essential features of convection patterns and their instabilities. The simplest model of this type is

$$\frac{\partial w}{\partial t}=[r-(1+\nabla^2)^2]w+N(w), \tag{18}$$

where $N(w)$ represents nonlinear terms and $w(x,y,t)$ represents the amplitude of the vertical velocity of convection after the dependence on z has been projected out. The model (18) is generally referred to as the Swift-Hohenberg equation, although it does not appear explicitly in the original paper of Swift and Hohenberg [14]. Certain simplifying as-

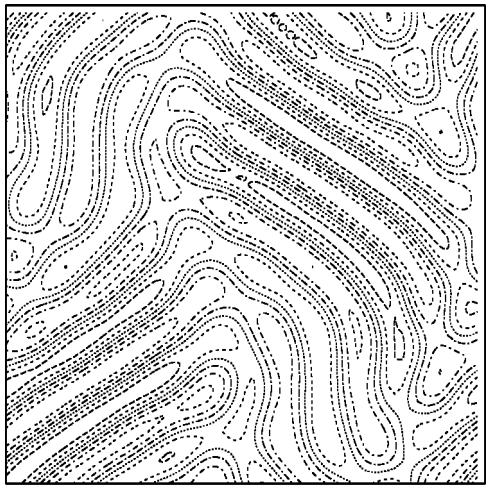

(a)

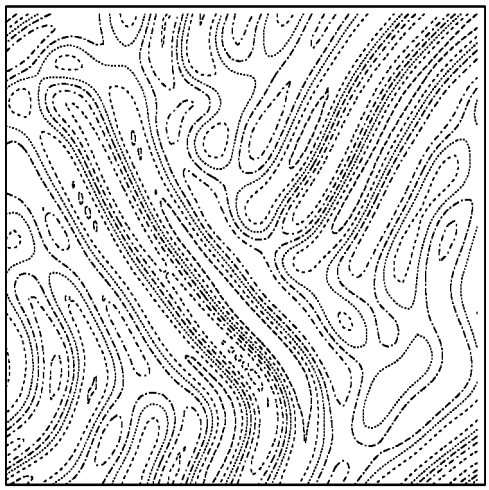

(b)

FIG. 4. Solutions for three-dimensional magnetoconvection with $\sigma=100, \zeta=0.7, Q=100$, showing contour plots of the vertical velocity w at the middle of the layer. (a): $R=2800$, contour interval =1. (b): $R=3000$, contour interval =2.

sumptions are necessary in any derivation of Eq. (18), and various different choices have been used for the nonlinear term $N(w)$. For convection at finite Prandtl number with stress-free boundaries, a stream function ψ representing a large-scale flow should be introduced as a second independent mode, because the linearized equation for this mode is the diffusion equation

$$\frac{\partial \psi}{\partial t} = \sigma \nabla^2 \psi, \tag{19}$$

and so this mode is only very weakly damped on large scales. This leads to a model in which Eq. (19) is coupled to Eq. (18) through nonlinear terms [15].

To derive a model for magnetoconvection we must include an eigenmode representing the rearrangement of the vertical magnetic field lines. The linearized equation for this mode is, from Eq. (3), the diffusion equation

$$\frac{\partial B}{\partial t} = \zeta \nabla^2 B, \tag{20}$$

so the growth rate λ of this mode is as given by Eq. (17). Our aim is to construct a system of two equations for w and B, which will take the form of Eqs. (18) and (20) with nonlinear coupling terms. To avoid the additional complications of the large-scale flow, which would lead to a system of three coupled equations, we take the limit of infinite Prandtl number.

We suppose that the convection is close to onset and introduce a small parameter ϵ such that

$$R = R_c + \epsilon^2 R_2, \tag{21}$$

where $R_2 = O(1)$. The amplitude of convective velocity w is then of order ϵ and we anticipate that the mean vertical magnetic field B is of order ϵ^2 since it should be unaffected by a sign change in w. Time derivatives are also of order ϵ^2. We derive our model equations in two steps: first we compute the appropriate linear terms in the evolution equation for w; then, we compute the nonlinear terms in this equation and the equation for B. To accomplish the first of these steps, we begin by linearizing the governing equations (1)–(4), then eliminating θ and B_z from $\hat{\mathbf{z}} \cdot \boldsymbol{\nabla} \times \boldsymbol{\nabla} \times (1)$ using Eqs. (2) and (3). The result is a linearized evolution equation for $w \propto \epsilon \sin \pi z$ in the form

$$\left(\frac{\partial}{\partial t} - \zeta \nabla^2\right)\left(\frac{\partial}{\partial t} - \nabla^2\right)\nabla^4 w = -R\nabla_H^2 \left(\frac{\partial}{\partial t} - \zeta \nabla^2\right) w + \pi^2 \zeta Q \left(\frac{\partial}{\partial t} - \nabla^2\right)\nabla^2 w. \tag{22}$$

If we now make the substitution (21) and assume that time derivatives are of order ϵ^2 and that $\mathcal{L} \equiv \nabla^2 + a_c^2 = O(\epsilon)$, as is appropriate for patterns with horizontal wave number $k \approx k_c$, we find at $O(\epsilon^3)$ in Eq. (22) that

$$\left(a_c^4 + \frac{Q(\zeta - 1)\pi^2}{\zeta}\right)\frac{\partial w}{\partial t} = (R_2 k_c^2 - 3a_c^2 \mathcal{L}^2) w. \tag{23}$$

To carry out the second step in the calculation, generating the nonlinear terms for Eq. (23) and the equation for B, the variables are expanded as

$$u = \epsilon u_1 \cos \pi z + \epsilon^2 u_2 \cos 2\pi z + \cdots, \tag{24}$$

$$v = \epsilon v_1 \cos \pi z + \epsilon^2 v_2 \cos 2\pi z + \cdots, \tag{25}$$

$$w = \epsilon w_1 \sin \pi z + \epsilon^2 w_2 \sin 2\pi z + \cdots, \tag{26}$$

$$\theta = \epsilon \theta_1 \sin \pi z + \epsilon^2 \theta_2 \sin 2\pi z + \cdots, \tag{27}$$

$$B_x = \epsilon B_{x1} \sin \pi z + \epsilon^2 B_{x2} \sin 2\pi z + \cdots, \tag{28}$$

$$B_y = \epsilon B_{y1} \sin \pi z + \epsilon^2 B_{y2} \sin 2\pi z + \cdots, \tag{29}$$

$$B_z = \epsilon B_{z1} \cos \pi z + \epsilon^2 B + \epsilon^2 B_{z2} \cos 2\pi z + \cdots, \quad (30)$$

where all the coefficients of the trigonometric functions of z are functions of x, y, and t only.

From this point on, we use ∇ and ∇^2 to denote the two-dimensional (horizontal) gradient operator and Laplacian, respectively, in order to simplify the notation. Where we use the corresponding three-dimensional operators, we henceforth denote these explicitly as ∇_{3D} and ∇_{3D}^2.

By considering terms at order ϵ in Eq. (2) we obtain

$$0 = w_1 + (\nabla^2 - \pi^2)\theta_1. \quad (31)$$

The components of Eq. (3) yield

$$0 = -\pi u_1 + \zeta(\nabla^2 - \pi^2)B_{x1}, \quad (32)$$

$$0 = -\pi v_1 + \zeta(\nabla^2 - \pi^2)B_{y1}, \quad (33)$$

$$0 = \pi w_1 + \zeta(\nabla^2 - \pi^2)B_{z1}, \quad (34)$$

and by combining $\hat{\boldsymbol{z}} \cdot \nabla_{3D} \times (1)$ with $\nabla_{3D} \cdot \boldsymbol{u} = 0$ it can be shown that

$$\nabla^2 u_1 = -\pi \frac{\partial w_1}{\partial x}, \quad (35)$$

$$\nabla^2 v_1 = -\pi \frac{\partial w_1}{\partial y}. \quad (36)$$

Hence all the linear quantities can be expressed in terms of w_1. Substituting these expressions into $\hat{\boldsymbol{z}} \cdot \nabla_{3D} \times \nabla_{3D} \times (1)$ and setting $\nabla^2 = -k^2$ gives the result (6) for the marginal stability curve.

At order ϵ^2, by evaluating the nonlinear terms in Eq. (2), $\hat{\boldsymbol{z}} \cdot (3)$, and $\hat{\boldsymbol{z}} \cdot \nabla_{3D} \times (1)$, it is found that the second-order functions w_2, θ_2, and B_{z2} are determined from

$$w_2 + (\nabla^2 - 4\pi^2)\theta_2 = \frac{\pi}{2k_c^2 a_c^2} M, \quad (37)$$

$$2\pi w_2 + \zeta(\nabla^2 - 4\pi^2)B_{z2} = 0, \quad (38)$$

$$R_c \nabla^2 \theta_2 - 2\pi\zeta Q(\nabla^2 - 4\pi^2)B_{z2} + (\nabla^2 - 4\pi^2)^2 w_2 = \frac{Q\pi^3}{2\zeta k_c^4 a_c^2} \nabla^2 M, \quad (39)$$

where

$$M = k_c^2 w_1^2 + |\nabla w_1|^2. \quad (40)$$

Now the system (37)–(39) cannot be solved exactly, since we do not know the form of M. However, for magnetoconvection it is known that convection takes the form of two-dimensional rolls at onset [25], and for convection in the form of rolls, so that $w_1 = W \cos(kx)$, for instance, M takes the constant value $M = k^2 W^2$. Assuming that convection forms a pattern that locally is close to regular rolls, we make the approximation that M is a constant. This approximation is consistent with the simulations of the full magnetoconvection problem shown in Fig. 4. In this case, the solution at second order is

$$\theta_2 = -\frac{M}{8\pi k_c^2 a_c^2}, \quad (41)$$

and $w_2 = B_{z2} = 0$, with B as yet undetermined. Note that we do not evaluate the "linear" correction terms that arise at this order, since their influence is entirely accounted for by the linear terms derived in Eq. (23).

We shall see below, in Sec. VI, that the assumption of constant M is too drastic and that in order to saturate the growth of localized convective states we must modify the model equations derived in this section to account for slow variations in M (see the Appendix). A more comprehensive model, in which the spatial dependence of M is retained, leading to more complicated nonlinear terms, is given in detail in [26]. However, for the moment, we retain the constant-M approximation.

At order ϵ^3, we obtain the relevant nonlinear terms in the evolution equation for w_1 by considering terms proportional to $\sin \pi z$ in $\hat{\boldsymbol{z}} \cdot \nabla_{3D} \times \nabla_{3D} \times (1)$ and (2), and terms proportional to $\cos \pi z$ in $\hat{\boldsymbol{z}} \cdot (3)$. We further make the assumption that the convective structures formed have horizontal wave number roughly k_c, and hence make the replacement $\nabla^2 \mapsto -k_c^2$. The relevant terms are then, respectively,

$$0 = R_c k_c^2 \theta_3 - \zeta Q a_c^2 \pi B_{z3} - a_c^4 w_3 + \frac{Q\pi^4}{a_c^2 k_c^2} \nabla \cdot (B \nabla w_1) - \frac{Q\pi^2}{a_c^2}(\nabla w_1 \cdot \nabla B + k_c^2 w_1 B), \quad (42)$$

together with

$$\frac{1}{a_c^2}\frac{\partial w_1}{\partial t} - w_3 + a_c^2 \theta_3 = -\frac{1}{8k_c^2 a_c^2} M w_1, \quad (43)$$

$$\frac{\pi}{\zeta a_c^2}\frac{\partial w_1}{\partial t} - \pi w_3 + \zeta a_c^2 B_{z3} = -\frac{\pi}{k_c^2} \nabla \cdot (B \nabla w_1), \quad (44)$$

where w_3, θ_3, and B_{z3} are the order-ϵ^3 terms with the same z dependence as the order-ϵ terms in the expansions (26), (27), and (30). Now multiplying Eq. (42) by a_c^2, Eq. (43) by $R_c k_c^2$, and Eq. (44) by $-Q\pi a_c^2$ and adding the resulting expressions together gives, after reinstating the linear terms from Eq. (23),

$$\left(a_c^4 + \frac{Q(\zeta - 1)\pi^2}{\zeta}\right)\frac{\partial w_1}{\partial t} = (R_2 k_c^2 - 3a_c^2 \mathcal{L}^2) w_1 + N_1, \quad (45)$$

where the nonlinear term N_1 can be written in terms of w_1 and B as

$$N_1 = -\frac{R_c}{8a_c^2} M w_1 - Q\pi^2(\boldsymbol{\nabla} w_1 \cdot \boldsymbol{\nabla} B + k_c^2 w_1 B) + \frac{Q\pi^2(2\pi^2 + k_c^2)}{k_c^2} \boldsymbol{\nabla} \cdot (B \boldsymbol{\nabla} w_1). \quad (46)$$

In view of the assumed z dependence of the leading-order contribution to w, the definition of $\mathcal{L}$ appropriate here is $\mathcal{L} = \nabla^2 + k_c^2$ (this is equivalent to the earlier definition of $\mathcal{L}$ as $\nabla_{3D}^2 + a_c^2$).

To complete the model we require an equation for the depth-averaged vertical magnetic field B. The linear terms are given in Eq. (20) and the nonlinear terms arise from those in the z component of the induction equation (3):

$$N_2 \equiv \left\langle \frac{\partial}{\partial x}(wB_x - uB_z) + \frac{\partial}{\partial y}(wB_y - vB_z) \right\rangle_z, \quad (47)$$

where $\langle \cdots \rangle_z$ denotes an average over z. Since the terms describing the large-scale magnetic field in Eq. (20) are of order ϵ^4, care must be taken in the evaluation of the terms in N_2; simply using Eqs. (32)–(36) with ∇^2 replaced by $-k_c^2$ to express N_2 in terms of w is not sufficiently accurate. We rewrite the nonlinear term by introducing poloidal potentials for the leading-order contributions to $\boldsymbol{u}$ and $\boldsymbol{B}$,

$$\boldsymbol{u} = \boldsymbol{\nabla}_{3D} \times \boldsymbol{\nabla}_{3D} \times (\phi \sin \pi z \hat{\boldsymbol{z}}) = (\phi_x \pi \cos \pi z, \phi_y \pi \cos \pi z, -\nabla^2 \phi \sin \pi z), \quad (48)$$

$$\boldsymbol{B} = \boldsymbol{\nabla}_{3D} \times \boldsymbol{\nabla}_{3D} \times (\psi \cos \pi z \hat{\boldsymbol{z}}) = (-\psi_x \pi \sin \pi z, -\psi_y \pi \sin \pi z, -\nabla^2 \psi \cos \pi z), \quad (49)$$

which correctly describe the $O(\epsilon)$ terms if $\phi = \epsilon w_1 / k_c^2$ and $\psi = \epsilon B_{z1} / k_c^2$. In this formulation the nonlinear term N_2 becomes

$$N_2 = \frac{\pi}{2}[(\nabla^2 \phi\ \psi_x + \nabla^2 \psi\ \phi_x)_x + (\nabla^2 \phi\ \psi_y + \nabla^2 \psi\ \phi_y)_y] = \frac{\pi}{2} \boldsymbol{\nabla} \cdot (\nabla^2 \phi\ \boldsymbol{\nabla} \psi + \nabla^2 \psi\ \boldsymbol{\nabla} \phi), \quad (50)$$

where the factor of $1/2$ arises from averaging in z the terms in $\sin^2 \pi z$ and $\cos^2 \pi z$. Now it can be shown that in this form, N_2 can be written as

$$N_2 = \frac{\pi}{2}\left\{ \left(\frac{\partial^2}{\partial x^2} - \frac{\partial^2}{\partial y^2} \right)(\phi_x \psi_x - \phi_y \psi_y) + 2\frac{\partial^2}{\partial x\, \partial y}(\phi_x \psi_y + \phi_y \psi_x) \right\}, \quad (51)$$

showing that each nonlinear term is subject to two derivatives. Therefore the mean component of N_2, on large scales in which horizontal derivatives are of order ϵ, is of order ϵ^4, as required for the large-scale mode B. Hence we may use the leading-order approximations $\phi = \epsilon w_1 / k_c^2$ and $\psi = \epsilon B_{z1} / k_c^2 = \epsilon \pi w / \zeta a_c^2 k_c^2$ in the formula (50) for N_2 to obtain the equation for B in the form

$$B_t = \zeta \nabla^2 B + \frac{\pi^2}{\zeta a_c^2 k_c^4} \boldsymbol{\nabla} \cdot (\nabla^2 w_1 \boldsymbol{\nabla} w_1). \quad (52)$$

To write the model system in a simpler form we rescale Eqs. (45) and (52) by introducing $(x', y') = (k_c x, k_c y)$, $t' = k_c^2 t$, $w' = \mathcal{W} w_1$, and $B' = \mathcal{W}^2 B$, where $\mathcal{W} = (a_c^2 / 12\pi^2 k_c^2)^{1/2}$. If all primes are then dropped, the resulting scaled system is

$$\tau_0 w_t = [r - (1 + \nabla^2)^2] w - w(w^2 + \boldsymbol{\nabla} w \cdot \boldsymbol{\nabla} w) - \alpha_2(wB + \boldsymbol{\nabla} w \cdot \boldsymbol{\nabla} B) + \alpha_3 \boldsymbol{\nabla} \cdot (B \boldsymbol{\nabla} w), \quad (53)$$

$$B_t = \zeta \nabla^2 B + \alpha_1 \boldsymbol{\nabla} \cdot (\nabla^2 w \boldsymbol{\nabla} w), \quad (54)$$

where the parameters are readily found to be

$$r = \frac{2a_c^4}{3k_c^2 \pi^2}\left(\frac{R - R_c}{R_c} \right),$$

$$\tau_0 = \frac{1}{3a_c^2 k_c^2}\left(a_c^4 + \frac{Q(\zeta - 1)\pi^2}{\zeta} \right),$$

$$\alpha_1 = \frac{\pi^2}{\zeta a_c^2 k_c^2} > 0,$$

$$\alpha_2 = 4(2k_c^2 - \pi^2) > 0, \quad (55)$$

$$\alpha_3 = \left(1 + \frac{2\pi^2}{k_c^2} \right)\alpha_2 > 0; \quad (56)$$

we have used Eqs. (7) and (8) to eliminate R_c and Q from the nonlinear coefficients α_1, α_2, and α_3. For Eq. (53) to be well posed, we need $\tau_0 > 0$—i.e., $\zeta > 1 - \pi^2 / 2k_c^2$. [Alternatively, we may write this condition as $\zeta \geqslant 1$ or $Q < \pi^2(3 - 2\zeta)^2 \zeta / 4(1 - \zeta)^3$.]

The model consists of a Swift-Hohenberg equation (53) coupled through nonlinear terms to an equation (54) for the mean vertical magnetic field B. Note that in this system, the horizontal average of B is conserved, according to Eq. (54). In view of the discussion following Eq. (16), the system (53), (54) is subject to the condition

$$\langle B \rangle_{x,y} = 0, \quad (57)$$

where $\langle \cdots \rangle_{x,y}$ denotes the horizontal spatial average.

V. ANALYSIS OF THE MODEL

In this section we analyze the behavior of solutions to the model equations (53) and (54) for w and B, near the onset of convection, concentrating on solutions in the form of rolls and their instabilities.

A. Linear stability of the conduction state

In the system (53) and (54), the conduction state $w = B = 0$ has two associated branches of eigenvalues corresponding to infinitesimal disturbances in either w or B:

$$w \sim \exp(\lambda t + i\boldsymbol{k}\cdot\boldsymbol{x}), \quad \tau_0\lambda = r - (1-k^2)^2, \tag{58}$$

and, as indicated in Eq. (17),

$$B \sim \exp(\lambda t + i\boldsymbol{k}\cdot\boldsymbol{x}), \quad \lambda = -\zeta k^2, \tag{59}$$

where $k=|\boldsymbol{k}|$. Thus the "pattern" branch, corresponding to disturbances in w, has maximum growth rate in this scaling at unit wave number: the conduction state is unstable for $r>0$, to a band of wave numbers $k\approx 1$. The second, "large-scale," branch does not itself directly give rise to any linear instability of the conduction state; nevertheless, it plays a significant role in pattern formation, which is made clear in the weakly nonlinear analysis that now follows.

B. Weakly nonlinear expansion

Near the onset of instability of the conduction state, we expand

$$w \sim \delta w_1 + \delta^2 w_2 + \cdots, \tag{60}$$

$$B \sim \delta^2 B_2 + \cdots, \tag{61}$$

where

$$r = \delta^2 r_2. \tag{62}$$

We examine the weakly nonlinear development of rolls with critical wave number, modulated on the spatial and temporal scales

$$(\mathcal{X},\mathcal{Y},\mathcal{T}) = (\delta x, \delta y, \delta^2 t). \tag{63}$$

Upon substituting these expansions into Eqs. (53) and (54) and considering the terms at $O(\delta)$, we choose

$$w_1 = \mathcal{A}(\mathcal{X},\mathcal{Y},\mathcal{T})e^{ix} + \text{c.c.}$$

for some complex envelope function $\mathcal{A}(\mathcal{X},\mathcal{Y},\mathcal{T})$. Correspondingly,

$$B_2 = \frac{\alpha_1}{2\zeta}(\mathcal{A}^2 e^{2ix} + \text{c.c.}) + \mathcal{G}(\mathcal{X},\mathcal{Y},\mathcal{T}),$$

where $\mathcal{G}(\mathcal{X},\mathcal{Y},\mathcal{T})$ represents a large-scale magnetic field. Amplitude equations governing the evolution of $\mathcal{A}$ and $\mathcal{G}$ arise from solvability conditions at $O(\delta^3)$ and $O(\delta^4)$, in Eqs. (53) and (54), respectively. These are

$$\tau_0\mathcal{A}_\mathcal{T} = r_2\mathcal{A} + 4\mathcal{A}_{\mathcal{X}\mathcal{X}} - b\mathcal{A}|\mathcal{A}|^2 - (\alpha_2+\alpha_3)\mathcal{A}\mathcal{G},$$

$$\mathcal{G}_\mathcal{T} = \zeta(\mathcal{G}_{\mathcal{X}\mathcal{X}} + \mathcal{G}_{\mathcal{Y}\mathcal{Y}}) + \alpha_1\left(|\mathcal{A}|^2_{\mathcal{X}\mathcal{X}} - |\mathcal{A}|^2_{\mathcal{Y}\mathcal{Y}}\right),$$

where

$$b = 4 + \frac{(3\alpha_2-\alpha_3)\alpha_1}{2\zeta} = 4\left[1 + \frac{\pi^2(k_c^2-\pi^2)(2k_c^2-\pi^2)}{\zeta^2 k_c^4(\pi^2+k_c^2)}\right]. \tag{64}$$

We assume that $b>0$, so that the rolls branch supercritically. This condition is satisfied for all ζ if $Q>4\pi^2$ or provided ζ is sufficiently large if $Q<4\pi^2$.

By rescaling $\mathcal{X}$, $\mathcal{Y}$, $\mathcal{T}$, $\mathcal{A}$, and $\mathcal{G}$, we may reduce these equations (in the interesting case $r_2>0$) to the canonical form

$$A_T = A + A_{XX} - A|A|^2 - AG, \tag{65}$$

$$G_T = s(G_{XX}+G_{YY}) + \mu(|A|^2_{XX} - |A|^2_{YY}), \tag{66}$$

with $\langle G\rangle_{X,Y}=0$, where the only remaining parameters are

$$s = \frac{\tau_0\zeta}{4} > 0, \quad \mu = \frac{\tau_0\alpha_1(\alpha_2+\alpha_3)}{4b} \gtrless 0. \tag{67}$$

C. Modulational stability of rolls

Roll solutions of Eqs. (53) and (54) with near-critical wave number correspond to solutions of Eqs. (65) and (66) of the form

$$A = A_0 e^{iKX}, \quad G = 0,$$

where $|A_0|^2=(1-K^2)$. The stability of these rolls is determined by considering perturbations in the form

$$A = A_0[1+\alpha(X,Y,T)]e^{iKX}, \quad G = \gamma(X,Y,T),$$

where $|\alpha|, |\gamma| \ll 1$. Since the linearized equations governing α and γ have spatially uniform coefficients, it suffices to investigate individual Fourier modes

$$\alpha = Ue^{i(lX+mY)} + V^* e^{-i(lX+mY)},$$

$$\gamma = We^{i(lX+mY)} + \text{c.c.},$$

where we note that γ is necessarily real valued, but α is in general complex. The amplitudes U, V, and W all have the same exponential T dependence, and the corresponding growth rate Λ satisfies a cubic equation, so there are three roots to be examined. The limit $l^2+m^2\to 0$ is of particular significance (although presumably instabilities may also arise at finite l or m). In this limit, one growth rate has $\Lambda \sim -2|A_0|^2<0$ and corresponds to the stability of rolls to uniform disturbances to their amplitude. The remaining two satisfy $\Lambda=O(l^2+m^2)$ and can be found from a quadratic equation, which in principle allows both monotonic and oscillatory instabilities. However, we have observed only the monotonic instability in simulations, so we focus on that case, finding that rolls are unstable if

$$s(l^2+m^2)(1-3K^2) + \mu(m^2-l^2)(1-K^2) < 0.$$

For a given value of l^2+m^2, the most dangerous disturbances have $m=0$, and hence there is instability to *one-dimensional* modulations if

$$s(1-3K^2) < \mu(1-K^2).$$

All rolls are thus unstable if [13]

$$\mu/s > 1. \tag{68}$$

In terms of the original parameters, we find that

$$\frac{\mu}{s} - 1 = \frac{\pi^2(2k^2 - \pi^2)(k^2 + 3\pi^2) - \zeta^2(k^2 + \pi^2)k^4}{\pi^2(2k^2 - \pi^2)(k^2 - \pi^2) + \zeta^2(k^2 + \pi^2)k^4},$$

and so all rolls are unstable for

$$\frac{\pi^2(2k^2 - \pi^2)(k^2 + 3\pi^2)}{(k^2 + \pi^2)k^4} > \zeta^2. \tag{69}$$

This result exactly recovers the stability boundary obtained from the full governing equations [7].

The stability of rolls to the zigzag instability is, to leading order, unaffected by the presence of the large-scale magnetic field: a standard weakly nonlinear analysis predicts that, near onset, rolls are unstable to zigzags if their wave number is less than critical (i.e., if $k<1$). A detailed analysis is not presented here but is given by Pollicott [26].

VI. NONLINEAR DEVELOPMENT OF THE MODULATIONAL INSTABILITY

The instability of rolls to modulation of their amplitude, as described above, was first discussed by Matthews and Cox [13]. The nonlinear development of this instability in large domains requires a delicate analysis, first given by Proctor [27], which reveals how the saturation of the instability depends on the parameters of the problem. In this section we derive a nonlinear amplitude equation that governs the instability, in the form derived by Proctor, and examine its evolution for the model (53), (54).

We consider Eqs. (53) and (54) in one space dimension, with $r=\delta^2 r_2$. As in Sec. V B, we expand w and B in the form (60), (61). To decide the direction of the bifurcation to modulation, it proves necessary to examine very wide boxes, and so instead of Eq. (63) we introduce modulational scales [27]

$$\mathcal{T}_6 = \delta^6 t, \quad \mathcal{X}_2 = \delta^2 x. \tag{70}$$

The analysis below holds near the onset of the modulational instability, and it is convenient to take α_1 as a tuning parameter to achieve this. We thus write

$$\alpha_1 = \alpha_{10}(1 + \delta^2 \alpha_{12}), \tag{71}$$

where, in view of Eqs. (64), (67), and (68), the threshold is

$$\alpha_{10} = \frac{8\zeta}{3\alpha_3 - \alpha_2}. \tag{72}$$

We now systematically consider Eqs. (53) and (54) at successive orders in δ. At $O(\delta^1)$, we write

$$w_1 = \mathcal{R}(e^{i(x+\Phi)} + e^{-i(x+\Phi)}), \tag{73}$$

where $\mathcal{R}=\mathcal{R}(\mathcal{X}_2,\mathcal{T}_6)$ and $\Phi=\Phi(\mathcal{X}_2,\mathcal{T}_6)$, and we define $\kappa_0(\mathcal{X}_2,\mathcal{T}_6)$ and $\kappa_2(\mathcal{X}_2,\mathcal{T}_6)$ by

$$\frac{\partial \Phi}{\partial \mathcal{X}_2} \sim \kappa_0 + \delta^2 \kappa_2. \tag{74}$$

At $O(\delta^2)$, we find

$$B_2 = \frac{4\mathcal{R}^2}{3\alpha_3 - \alpha_2}(e^{2i(x+\Phi)} + e^{-2i(x+\Phi)}) + B_{20}, \tag{75}$$

where $B_{20}(\mathcal{X}_2,\mathcal{T}_6)$ is, as yet, unknown. At $O(\delta^3)$, we find

$$w_3 = -\frac{\mathcal{R}^3}{16}(e^{3i(x+\Phi)} + e^{-3i(x+\Phi)}) + \mathcal{R}_2(e^{i(x+\Phi)} + e^{-i(x+\Phi)}), \tag{76}$$

where $\mathcal{R}_2(\mathcal{X}_2,\mathcal{T}_6)$ is for the moment arbitrary. In addition, from the terms in Eq. (53) proportional to $e^{\pm i(x+\Phi)}$, we find that

$$B_{20} = \frac{1}{\alpha_3 + \alpha_2} - \frac{8\mathcal{R}^2}{3\alpha_3 - \alpha_2}. \tag{77}$$

Thus, in view of Eq. (57),

$$\langle \mathcal{R}^2 \rangle = \frac{3\Xi - 1}{8(\Xi + 1)}, \tag{78}$$

where we have introduced

$$\Xi = \frac{\alpha_3}{\alpha_2}. \tag{79}$$

The remainder of the calculation is rather algebraically involved, so we note here only the structure of the results at the various orders in δ. At $O(\delta^4)$, we find B_4, up to its spatial average, $B_{40}\equiv\langle B_4\rangle$. At $O(\delta^5)$, we find, from the imaginary part of the coefficient of $e^{i(x+\Phi)}$ in Eq. (53), that κ_0 takes the form

$$\kappa_0 = \frac{h(\mathcal{T}_6)}{\mathcal{R}^2} - \frac{\Xi}{4(\Xi + 1)} + \frac{3(9\Xi - 7)\mathcal{R}^2}{8(3\Xi - 1)} \tag{80}$$

for some $h(\mathcal{T}_6)$; from the corresponding real part of this coefficient, we find a (rather complicated) expression for B_{40}. It follows from Eq. (80) that

$$h\langle \mathcal{R}^{-2} \rangle = \langle \kappa_0 \rangle + \frac{21 - 11\Xi}{64(\Xi + 1)}. \tag{81}$$

We also find a complicated expression for w_5. At $O(\delta^6)$, the solution is complicated and sheds little light on the calculation at hand. The problem at $O(\delta^7)$ yields equations for $\mathcal{R}_2$ and κ_2 upon consideration of the real and imaginary parts of the coefficient of $e^{i(x+\Phi)}$, respectively. These expressions are not, however, necessary for the present calculation.

Finally, at $O(\delta^8)$, consideration of the spatial average of Eq. (54) yields the evolution equation

$$\mathcal{R}\frac{\partial \mathcal{R}}{\partial \mathcal{T}_6} = \frac{\delta^2}{\partial \mathcal{X}_2^2}\left[-\frac{2\zeta\langle \mathcal{R}^2 \rangle}{\mathcal{R}}\left(\frac{\delta^2 \mathcal{R}}{\partial \mathcal{X}_2^2} - \frac{h^2}{\mathcal{R}^3}\right) + c\mathcal{R}^2 + d\mathcal{R}^4 \right], \tag{82}$$

where

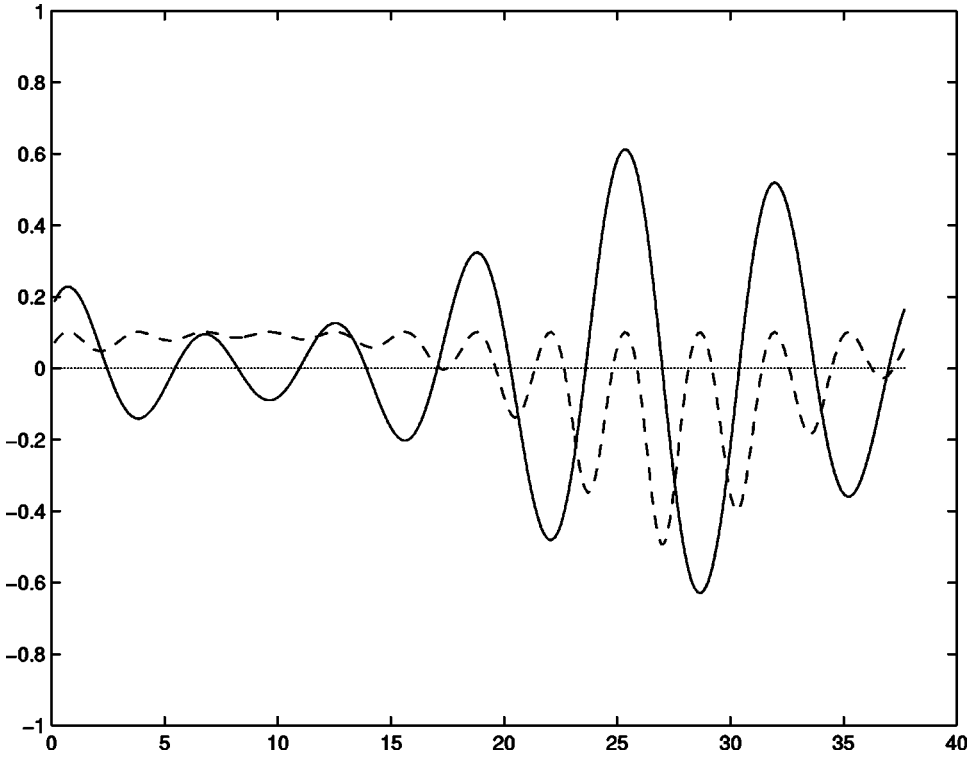

FIG. 5. Stable solution to the model equations (53) and (54) in one dimension, for $Q=100$,$L=12\pi$,$\zeta=1.0$. Solid line: w. Dashed line: $100B$.

$$c = \frac{\zeta\Xi(21\Xi - 11)}{32(\Xi + 1)^2} - 2\zeta\langle\mathcal{R}^2\rangle\alpha_{12} \tag{83}$$

and

$$d = -\frac{\zeta(1719\Xi^2 - 2034\Xi + 535)}{256(3\Xi - 1)(\Xi + 1)}. \tag{84}$$

Thus the modulation of the pattern is governed by Eq. (82), subject to Eqs. (78) and (81).

Proctor's equation (82) predicts that in general the bifurcation from a uniform-amplitude state with $\mathcal{R}=[(3\Xi-1)/8(\Xi+1)]^{1/2}$ to an amplitude-modulated state is subcritical [27] (except in sufficiently small boxes). It is also capable of describing the nonlinear development of this instability. Since the sign of d determines whether an instability of moderate size saturates, it is more illuminating to substitute for Ξ, using Eqs. (55), (56), and (79), to give

$$d = -\frac{\zeta(1719\pi^4 + 702k^2\pi^2 + 55k^4)}{256a^2(k^2 + 3\pi^2)} < 0, \tag{85}$$

which reveals the term $d\mathcal{R}^4$ to be destabilizing in Eq. (82) [27]. This term then tends to lead to a blowup of solutions once $\mathcal{R}$ exceeds some (moderate) size. We find such a blowup quite generally in numerical simulations of Eqs. (53) and (54).

In fact, it is to be expected that the model (53), (54) should exhibit a blowup, for the following reason. The model incorporates the physical mechanisms of expulsion of a magnetic field from regions of stronger convection (through the α_1 term) and enhancement of convection in regions where the magnetic field is weaker (via the α_2 term). In the full system, this process continues until almost all of the magnetic field has been expelled from the regions of strong convection, as shown in Fig. 1, at which point the amplitude of convection can be increased no further. But in the reduced model, B represents the perturbation to the magnetic flux and can become arbitrarily large and negative.

To resolve the blowup, we recall that the model derived here is a simplified version of a more sophisticated model [26], in which M is not assumed to be constant at $O(\epsilon^2)$. The terms retained in the present model are sufficient to capture accurately the various stability boundaries of the rolls, but are evidently not sufficient to prevent the blowup of modulated states. To stabilize the model, we include terms from [26] corresponding to the "slowest" variations in M. Terms involving $\boldsymbol{\nabla}M$ are retained, but terms involving $\nabla^2 M$ are omitted. The resulting model derivation, summarized in the Appendix, maintains the relative simplicity of the present model by adding to the right-hand side of Eq. (53) a single additional term of the form

$$\alpha_4 \boldsymbol{\nabla} w \cdot \boldsymbol{\nabla} (w^2 + |\boldsymbol{\nabla} w|^2). \tag{86}$$

We emphasize that neither this nor any of the other omitted terms affects the stability boundaries of roll solutions. If we repeat the calculation above to determine the direction of the bifurcation, we find that the sign of d is then the same as that of

$$-(1719\pi^4 + 702k_c^2\pi^2 + 55k_c^4) + 4(31k_c^2 + 111\pi^2)(k_c^2 + 3\pi^2)\alpha_4 - 12(k_c^2 + 3\pi^2)^2\alpha_4^2.$$

We thus achieve a stabilization of the modulated state whenever $1.39 < \alpha_4 < 9.87$ (this interval yields $d>0$ for any $k^2 > \pi/2$).

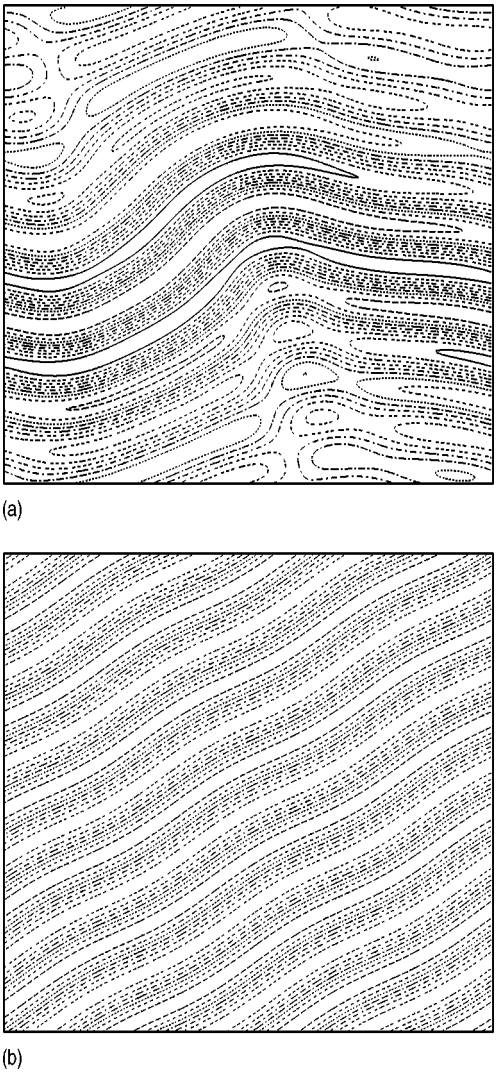

FIG. 6. Numerical solutions to the model equation (53) and (54) in two dimensions, showing contours of w, for $Q=100$, $L=12\pi$, $\zeta=1.0$, with a contour interval of 0.1. (a): modulated rolls at $t=750$. (b): stable wavy rolls, $t=3000$.

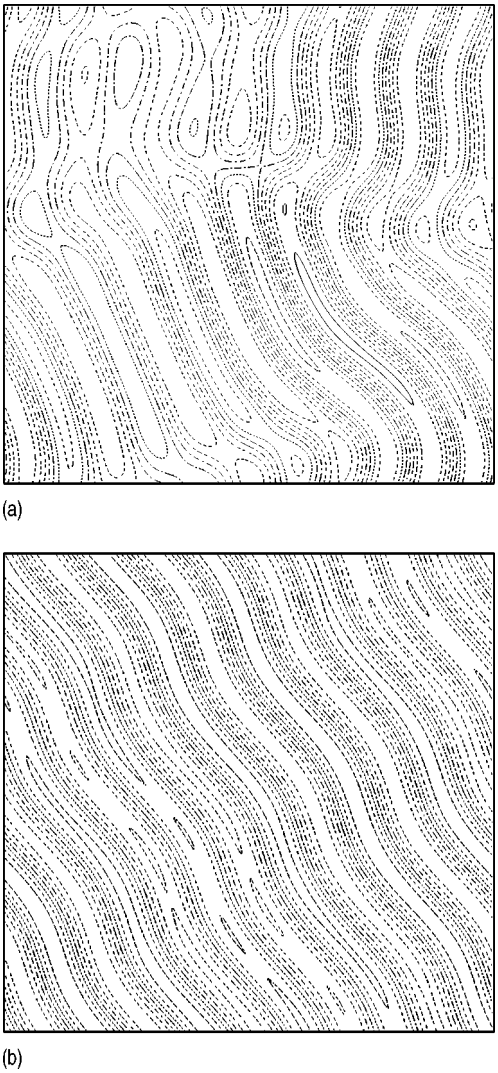

FIG. 7. Numerical solutions to the model equation (53) and (54) in two dimensions, showing contours of w, for $Q=100$,$L=12\pi$,$\zeta=0.8$. (a): transient modulated state at $t=700$. (b): stable modulated wavy rolls at $t=3000$.

VII. NUMERICAL SOLUTIONS OF THE MODEL

The model (53), (54) is solved numerically in a square periodic box $0\leqslant x,y\leqslant L$, where L is specified below. The code is pseudospectral, with the solutions for w and B expanded as Fourier series in x and y. The resulting nonlinear system of ordinary differential equations for the mode amplitudes is truncated at 256 modes in each direction. This system is stiff, largely due to the linear fourth derivative term appearing in Eq. (53), and time stepping is achieved using exponential time differencing [28], which is an efficient method for stiff systems. The initial condition is a small random perturbation to the equilibrium $w=B=0$ that satisfies the constraint (57).

Parameter values are chosen corresponding to $Q=100$, with $L=12\pi$, so that six pairs of rolls are contained in the domain, to allow comparison with the three-dimensional magnetoconvection simulations of Sec. III. The ratio $(R-R_c)/R_c$ is set to 0.05, which corresponds to $r=0.137$ in Eq. (53) and to $R\approx 2787$; thus the most appropriate comparison is with the three-dimensional simulations in Fig. 4 (at $R=2800$).

For $Q=100$, $k_c=3.70$ and so according to Eq. (69) rolls are unstable for $\zeta<\zeta_c=1.30$; however, the influence of the finite domain size reduces ζ_c to $\zeta_c\approx 1.06$.

According to the nonlinear analysis in Sec. VI, it is to be expected that solutions to the original model (53), (54) blow up for $\zeta<\zeta_c$. This is confirmed by the numerical solutions, which show that for $\zeta<\zeta_c$, rolls are unstable to amplitude modulation but this modulation increases without limit. To prevent this blowup, all the numerical solutions presented here incorporate the additional term $\alpha_4\boldsymbol{\nabla} w\cdot\boldsymbol{\nabla}(w^2+|\boldsymbol{\nabla} w|^2)$ on the right-hand side of Eq. (53), as discussed in Sec. VI and derived in the Appendix. The value $\alpha_4=2$ is found to be sufficient to keep the solutions finite, so this value is used throughout. Note that, as emphasized above, the α_4 term does not alter the value of ζ_c.

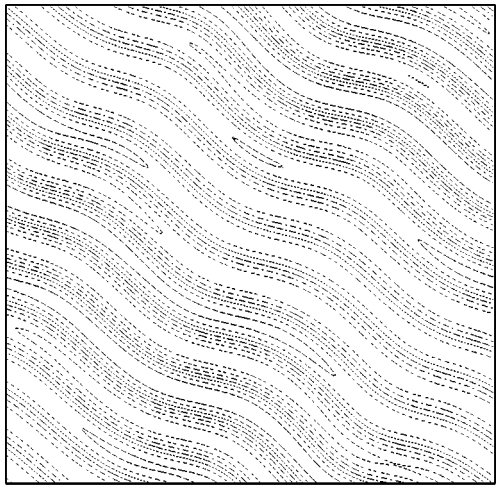

(a)

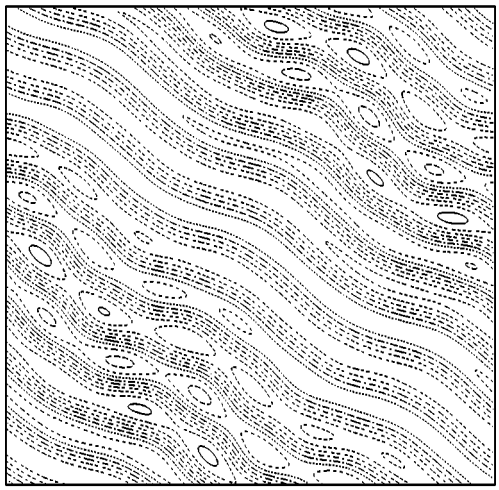

(b)

FIG. 8. Numerical solutions to the model equation (53) and (54) in two dimensions, showing contours of w, for $Q=100, L=12\pi, \zeta=0.7$. (a): modulated wavy rolls at $t=1000$. (b): $t=3000$.

A stationary solution in one dimension is shown in Fig. 5, for $\zeta=1$, in which case the other parameters in the model take the values $\tau_0=0.573$, $\alpha_1=0.0306$, $\alpha_2=70.13$, and $\alpha_3=171.2$. Here, w exhibits a strong modulation in its amplitude, while B (scaled up by a factor of 100 in the figure) is positive where w is weak and predominantly negative where w is strong, thus inhibiting or enhancing w through the $-\alpha_2 wB$ term in Eq. (53). For smaller values of ζ, a more strongly modulated, asymmetrical traveling wave packet is found.

In two dimensions, the above one-dimensional solutions are found to be unstable, and there appears to be a preference for wavy or zigzag rolls, as was found in the full magnetoconvection equations in Sec. III. Also, these wavy rolls seem to be less susceptible to the amplitude-modulation instability. As is to be expected for a complicated system in a large domain, more than one state can be obtained for the same parameter values, depending on the initial conditions.

A two-dimensional simulation with $\zeta=1$ (so that the parameters are the same as in Fig. 5) is shown in Fig. 6. Initially, a pattern of rolls forms, and these rolls become unstable to a modulation of their amplitude. However, these modulated rolls are unstable to a buckling mode and become strongly kinked (Fig. 6, left). After some further transient behavior, the system reaches a stable state of wavy rolls which are not amplitude modulated (Fig. 6, right).

When ζ is reduced to 0.8, the model exhibits a long transient phase involving highly time-dependent patches of modulated rolls (Fig. 7), which is similar to the behavior shown in Fig. 4 for the full system. At large t, however, the model settles down to a state of wavy rolls with a slight modulation in their amplitude.

The results of a simulation with $\zeta=0.7$ are shown in Fig. 8. At $t=1000$ a pattern of wavy rolls is seen, modulated in amplitude in the direction transverse to the rolls. At larger times, some secondary structures appear along the axes of the rolls. This is not a stationary state, but the qualitative appearance remains the same as t increases further. In these solutions the amplitude of w in the strong regions is approximately twice that in the weak regions.

Further simulations in larger domains show a very similar behavior, with stable wavy rolls for ζ near ζ_c and modulated wavy rolls for smaller values of ζ. Because of the constraint $\tau_0>0$, it is not possible to investigate magnetoconvection for $\zeta<0.64$, with $Q=100$.

There is very good qualitative agreement between the results of the two-dimensional model (53), (54), shown in Figs. 6–8, and the three-dimensional magnetoconvection simulations shown in Fig. 4. Both systems exhibit wavy roll structures with moderate modulation of amplitude.

VIII. CONCLUSIONS

We have developed a two-dimensional model for magnetoconvection valid near onset, under conditions that give rise to stationary onset. The model is derived by factoring out the vertical dependence of the convection, and involves a Swift-Hohenberg-like equation for the planform of the vertical velocity component coupled to an equation governing large-scale redistribution of the magnetic field. Although large-scale variations in the magnetic field are linearly damped, they can tend to suppress the convection in some regions, where the local magnetic field strength is elevated, and promote convection where the magnetic field is correspondingly weaker. The full magnetoconvection problem and the reduced model provide an example of the instability to amplitude modulation of systems with a conserved quantity, discussed by Matthews and Cox [7,13] and Proctor [27].

The linear terms in our model are the same as for models of convection with stress-free boundaries, where a Swift-Hohenberg equation is coupled to an equation for the stream function ψ [15,17,19]. The nonlinear coupling terms, however, are different, since ψ changes sign under reflection but the magnetic field does not.

The model captures many features of the full magnetoconvection equations. In particular, the linear stability boundary of the conduction state and the secondary stability boundaries of the regular roll solution to modulational instabilities are captured exactly by the model. Further compari-

sons of the model with the full problem have been carried out through numerical simulations, in order to explore the phenomenon of flux separation [5,10]. In one horizontal dimension, both systems exhibit stationary, strongly modulated states. In two horizontal dimensions, the behavior is more complex and the one-dimensional modulated rolls appear to be unstable to a buckling mode. This can lead to stable, wavy unmodulated rolls, to stable, wavy modulated rolls, or to time-dependent modulated states. The behavior of the model shows good agreement with the simulations of the full equations at large Prandtl number.

This work raises several questions for future research. It is of interest to determine whether similar modulated states occur in the parameter regime where magnetoconvection is oscillatory at onset and whether a reduced model can be derived for this case. Other possible extensions include the case of finite Prandtl number, where there is an additional large-scale mode to be included [15], and the inclusion of the effects of compressibility.

APPENDIX: DERIVATION OF ADDITIONAL STABILIZING TERM IN THE MODEL

At $O(\epsilon^2)$ in the derivation of the model equation for w, we simplified matters by taking M to be independent of x and y. By making this assumption, we were then able straightforwardly to solve the equations for w_2, θ_2, and B_{z2}. If we remove this restriction on M and admit that it will in fact vary with x and y, then further analytical progress is not in general possible. One circumstance, however, in which progress can be made is if we adopt the approximation $k_c^2 \ll 4\pi^2$, so that we may neglect the ∇^2 terms on the left-hand sides of Eqs. (37)–(39) in comparison with the $-4\pi^2$ terms [15,17]. Such an approximation cannot be justified in general, but it might be acceptable when Q is not too large, since then $k_c \sim \pi/\sqrt{2}$ (so that this approximation corresponds to taking $1 \ll 8$). We note that some restriction on the magnitude of Q is in keeping with our expectation that the model will become inappropriate when Q is large enough for the oscillatory bifurcation to precede the stationary bifurcation from the conduction state.

If we make this approximation, then Eqs. (37) and (38) allow us to write θ_2 and B_{z2} in terms of w_2 and M as

$$\theta_2 = \frac{1}{4\pi^2}\left(w_2 - \frac{\pi M}{2k_c^2 a_c^2}\right), \quad B_{z2} = \frac{w_2}{2\pi\zeta}. \tag{A1}$$

Substituting these expressions into Eq. (39) and again replacing $\nabla^2 - 4\pi^2$ with $-4\pi^2$ in all cases, we obtain the following equation relating w_2, $\nabla^2 w_2$, and M:

$$\frac{R_c}{4\pi^2}\nabla^2 w_2 + 4\pi^2 Q w_2 + 16\pi^4 w_2 = \left(\frac{Q\pi^3}{2\zeta k_c^4 a_c^2} + \frac{R_c}{8\pi k_c^2 a_c^2}\right)\nabla^2 M.$$

Before we can find w_2, we need to make some further simplification. As in the earlier approximations, we neglect the $\nabla^2 w_2$ term compared with w_2 term, corresponding to the assumption that $R_c \ll (4\pi^2)^3$ (which, when Q is small, amounts to the reasonable assumption that $27 \ll 256\pi^2$). We then find

$$w_2 = \frac{a_c^4}{16\pi^5 k_c^2 (Q + 4\pi^2)}\left(1 + \frac{2Q\pi^6}{\zeta k_c^2 a_c^6}\right)\nabla^2 M.$$

The next stage is to obtain θ_2 and B_{z2} from Eq. (A1); additionally, in computing the former we make the approximation, consistent with our argument above, that we should neglect $\nabla^2 M$ compared with M, so that θ_2 remains as in Eq. (41). The final step at this order is to find (u_2, v_2) and (B_{x2}, B_{y2}). Equations exactly analogous to Eqs. (35) and (36) hold at second order, and from these it can be deduced that $(u_2, v_2) \propto \nabla M$, and similarly for (B_{x2}, B_{y2}).

Having calculated these additional terms at $O(\epsilon^2)$, we may then compute the corresponding terms at $O(\epsilon^3)$ in the equation for w_t. The details are rather algebraically cumbersome and unenlightening, but the principal change of interest is the introduction into the right-hand side of Eq. (45) of terms proportional to $\nabla w_1 \cdot \nabla M$ and $w_1 \nabla^2 M$. The latter is neglected, on the basis described above, as being much smaller than the retained term proportional to $w_1 M$, leaving the former term. Although a formula can be found for the coefficient α_4 of the $\nabla w_1 \cdot \nabla M$ term, in view of the large number of approximations required in this derivation we regard α_4 as a free parameter and have used the value $\alpha_4 = 2$ in the simulations of Sec. VII.

[1] S. Chandrasekhar, *Hydrodynamic and Hydromagnetic Stability* (Clarendon Press, Oxford, 1961).
[2] N. O. Weiss, J. Fluid Mech. **108**, 247 (1981).
[3] M. R. E. Proctor and N. O. Weiss, Rep. Prog. Phys. **45**, 1317 (1982).
[4] P. C. Matthews, M. R. E. Proctor, and N. O. Weiss, J. Fluid Mech. **305**, 281 (1995).
[5] L. Tao, N. O. Weiss, D. P. Brownjohn, and M. R. E. Proctor, Astrophys. J. Lett. **496**, L39 (1998).
[6] A. M. Rucklidge, N. O. Weiss, D. P. Brownjohn, P. C. Matthews, and M. R. E. Proctor, J. Fluid Mech. **419**, 283 (2000).
[7] S. M. Cox and P. C. Matthews, Physica D **149**, 210 (2001).
[8] F. Cattaneo, T. Emonet, and N. Weiss, Astrophys. J. **588**, 1183 (2003).
[9] S. M. Blanchflower, A. M. Rucklidge, and N. O. Weiss, Mon. Not. R. Astron. Soc. **301**, 593 (1998).
[10] N. O. Weiss, M. R. E. Proctor, and D. P. Brownjohn, Mon. Not. R. Astron. Soc. **337**, 293 (2002).
[11] S. M. Blanchflower, Phys. Lett. A **261**, 74 (1999).
[12] S. M. Blanchflower and N. O. Weiss, Phys. Lett. A **294**, 297 (2002).
[13] P. C. Matthews and S. M. Cox, Nonlinearity **13**, 1293 (2000).
[14] J. Swift and P. C. Hohenberg, Phys. Rev. A **15**, 319 (1977).
[15] P. Manneville, J. Phys. (Paris) **44**, 759 (1983).
[16] M. Neufeld, R. Friedrich, and H. Haken, Z. Phys. B: Condens. Matter **92**, 243 (1993).

[17] Y. Ponty, T. Passot, and P. L. Sulem, Phys. Rev. E **56**, 4162 (1997).
[18] Y. Ponty, T. Passot, and P. L. Sulem, Phys. Fluids **9**, 67 (1997).
[19] S. L. Pollicott, P. C. Matthews, and S. M. Cox, Phys. Rev. E **67**, 016301 (2003).
[20] R. C. Kloosterziel and G. F. Carnevale, J. Fluid Mech. **480**, 25 (2003).
[21] G. Dangelmayr, in *Dynamics of Nonlinear Waves in Dissipative Systems: Reduction, bifurcation and stability*, edited by G. Dangelmayr, B. Fiedler, K. Kirchgässner, and A. Mielke, Vol. 352 of *Pitman Research Notes in Mathematics Series* (Longman, Essex, England, 1996), pp. 5–78.
[22] S. M. Cox and P. C. Matthews, Int. J. Numer. Methods Fluids **25**, 151 (1997).
[23] B. Fornberg, *A Practical Guide to Pseudospectral Methods* (Cambridge University Press, Cambridge, England, 1998).
[24] S. M. Cox, SIAM (Soc. Ind. Appl. Math.) J. Appl. Math. **58**, 1338 (1998).
[25] T. Clune and E. Knobloch, Physica D **74**, 151 (1994).
[26] S. L. Pollicott, Ph.D. thesis, University of Nottingham, 2002.
[27] M. R. E. Proctor, Phys. Lett. A **292**, 181 (2001).
[28] S. M. Cox and P. C. Matthews, J. Comput. Phys. **176**, 430 (2002).